High-Precision Hugoniot Measurement of Aluminum up to 90 Mbar on the 100-kJ Laser Facility *

Wei-Ming Yang(杨为明), Xiao-Xi Duan(段晓溪), Xiao-Shi Peng(彭晓世), Zan-Yang Guan(关赞洋), Huan Zhang(章欢), Meng-Sheng Yang(杨蒙生), Ying-Hui Ren(任颖慧), Hao-Liu(刘浩), Dong-Xiao Liu(刘东晓), Yun-Song Dong(董云松), Chen Zhang(张琛), Zhi-Chao Li(李志超), Dong Yang(杨冬), Zhe-Bin Wang(王哲斌) * and Jia-Min Yang(杨家敏) **

[1]National Key Laboratory of Plasma Physics, Research Center of Laser Fusion, China Academy of Engineering Physics, Mianyang 621900, China

*Supported by the Science Challenge Project under Grant No. 2025013, the Foundation of National Key Laboratory of Plasma Physics under Grant No. JCKYS2025212803, JCKY2023212801, 6142A04230101 and the National Natural Science Foundation of China under Grant No. 12475239, 12275029, 1220527.
**Corresponding author. Email: zhebinw@vip.sina.com and yjm70018@sina.cn.

(xx April 2026)

Aluminum is the standard material for ultrahigh-pressure impedance-matching experiments, yet its principal Hugoniot above 50 Mbar, where inner-shell ionization dominates, lacks precise experimental data. Here we report laser-driven Hugoniot measurements of aluminum at 89 and 93 Mbar using an indirect-drive hohlraum on a 100-kJ laser facility. The shock velocities were determined with a combined uncertainty below 0.5% using a dual-diagnostic approach. With quartz as the impedance-matching standard, the measured compression ratios are 4.47±0.17 and 4.58±0.18. These results agree with models that include shell effects, including extended first-principles molecular dynamics, stochastic density functional theory, and the Hartree–Fock–Slater model with charged hard spheres, but deviate by 8–10% from average-atom models such as SESAME. These results validate shell-resolved equation-of-state models against average-atom predictions in the hundred-megabar regime, and provide a quantitative benchmark confirming that L-shell ionization softens the aluminum Hugoniot. This establishes a long-sought high-precision reference that supports aluminum as a standard for ultrahigh-pressure impedance matching.

Key words： Equation of state, standard material, impedance-matching, shell effects

PACS: 52.50.Lp, 62.50.Ef, 64.30.Jk, 52.57.-z

The equation of state (EOS) of materials at terapascal (TPa, 10 Mbar) pressures is fundamental for modeling planetary interiors [1-3], stellar evolution [4-5], and inertial confinement fusion implosions [6-10]. The impedance-matching technique is the most commonly used experimental method for determining Hugoniot states under such extreme conditions and is now widely implemented on various high-energy-density facilities [11-16]. Among all materials, aluminum (Al) serves as the primary standard for ultrahigh pressure impedance matching experiments due to its well characterized low pressure Hugoniot [17-18]. The reliability of Al's shock compression curve directly affects the accuracy of EOS data for many other materials, from iron in giant planet cores to ablator plastics in ICF targets.

The available Hugoniot data for aluminum, however, are unevenly distributed in pressure. Below about 5 Mbar, gas-gun, explosive, and magnetically driven flyer-plate experiments have

provided a large number of high-precision data points [19-22]. In this region, various theoretical models have been well tested and generally agree with one another [23-24]. At higher pressures, the situation changes markedly. Above approximately 10 Mbar, experimental data become sparse and are drawn mainly from underground nuclear tests [25-27]. Although these data extend the Hugoniot to several hundred megabars, the typical uncertainty in shock velocity exceeds 1.5%, which leads to considerable scatter in the derived density and pressure. This level of uncertainty is not sufficient to resolve the finer features expected from inner-shell ionization in the range of roughly 50 to 500 Mbar [28-30]. Kadatskiy and Khishchenko have pointed out that an experimental test of shell-induced oscillations in the aluminum Hugoniot would require a velocity measurement accuracy better than 0.5% [31], a level that has not yet been demonstrated for aluminum in this regime. A direct Hugoniot measurement with significantly improved precision is therefore needed to test these theoretical predictions and to establish a reliable benchmark in the shell-ionization regime. This gap undermines aluminum's reliability as an impedance-matching standard at hundreds of megabars, where it is most critically needed.

Theoretical predictions in this high-pressure region differ considerably. Models that include electronic shell structure explicitly, such as the Hartree-Fock-Slater model with charged hard spheres [30-31], density functional theory molecular dynamics [32-33], and path-integral Monte Carlo simulations [34], predict a softening of the Hugoniot as successive electron shells become ionized. In contrast, average-atom models based on Thomas-Fermi theory do not resolve shell effects and yield a stiffer Hugoniot with less structure [30,35]. The lack of high-precision data in the multi-TPa regime has prevented a definitive assessment of these competing descriptions, leaving the compressibility of aluminum under extreme conditions an open question. A direct Hugoniot measurement for aluminum with an uncertainty substantially lower than current data is therefore needed to test these theoretical predictions and to establish a reliable benchmark in the shell-ionization regime.

Here, we report a laser-driven Hugoniot measurement of aluminum at 93 Mbar with a shock-velocity measurement uncertainty below 0.5%. This result fills the critical experimental gap and provides a direct benchmark to validate shell-resolved EOS models.

The experiments were conducted on the 100kJ laser facility at the Laser Fusion Research Center [36]. A total of 45 beams delivered a 3 ns square pulse with energies between 124 and 133 kJ, irradiating the inner walls of a gold hohlraum. This generated an x-ray radiation drive with a temperature of ~270 eV, which launched a planar shock wave into a composite target attached to the hohlraum waist. The target assembly, illustrated in Fig. 1(a), consisted of a stepped aluminum sample thermally diffusion-bonded [37] to a quartz standard. The aluminum sample comprised a 190 μm-thick base and a 120 μm-thick step. A thin indium layer (~200 nm) was used for bonding, an order of magnitude thinner than typical micron-scale glue layers [11-13], so that no separate correction for the shock transit time was required. The initial densities were 2.7 g/cm³ for aluminum and 2.65 g/cm³ for quartz.

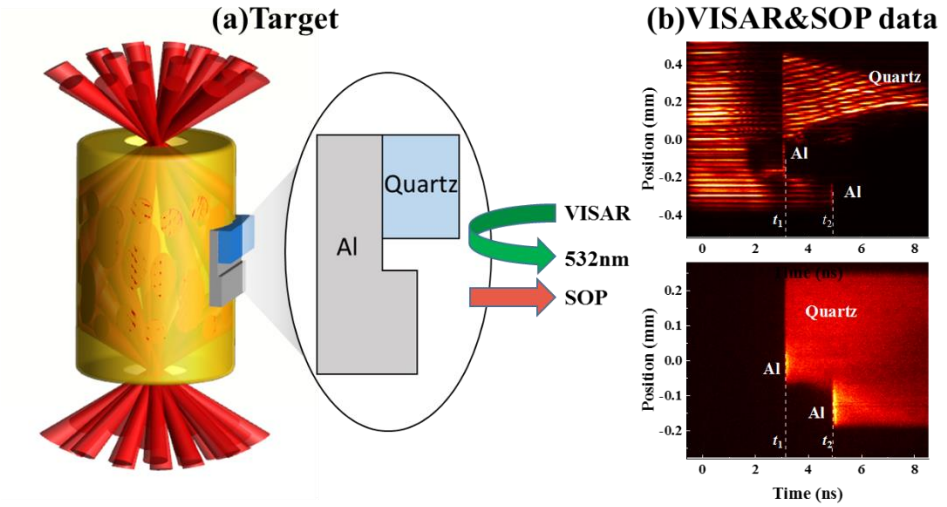


Fig. 1. (a) Schematic of the experimental setup. A gold hohlraum irradiated by 45 laser beams generates an x-ray drive that launches a planar shock into a composite target consisting of a stepped aluminum sample (190 μm base, 120 μm step) thermally diffusion-bonded to a quartz standard. (b) Raw streak records: upper panel shows VISAR fringes from the quartz standard; lower panel shows SOP self-emission from the aluminum rear surface. Breakout times from the base (t_1) and step (t_2) are marked.

Shock velocities were determined using a dual-diagnostic approach. The average shock speed in the opaque aluminum step was derived from the transit time between shock breakout from the base and the step, measured by a passive shock breakout diagnostic system (PSBO) [38]. Representative PSBO data [Fig. 1(b), lower panel] show the spatially and temporally resolved self-emission from the target rear surfaces. The breakout times t_1 (base) and t_2 (step) were identified from the steepest rise in intensity, with a combined temporal uncertainty of 12–27 ps. Simultaneously, the in-situ shock velocity history in the transparent quartz standard was recorded using a velocity interferometer system for any reflector (VISAR) [39] with a 532 nm probe laser [Fig. 1(b), upper panel]. The fringe shifts provide a continuous record of the shock velocity $D_{Qz}(t)$. The step thickness was characterized by dual confocal microscopy (DCM) over the diagnostic region; its uniformity was verified to better than 0.15 μm. Shock planarity was validated by a dedicated flat-foil shot, which gave a breakout-time fluctuation of less than 4 ps across 500 μm. Detailed descriptions of these procedures are provided in the Supplementary Material. The streak camera was calibrated to a relative timing precision of ~5 ps. These checks confirm that systematic contributions are well within the quoted uncertainties.

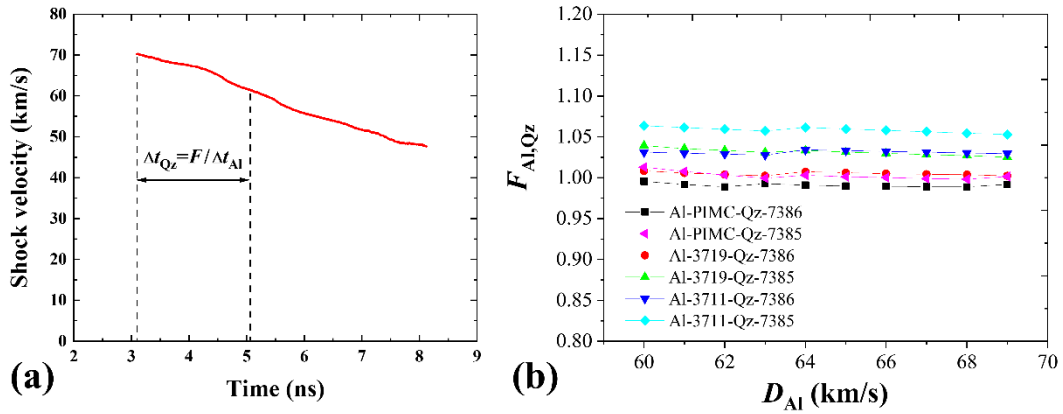


Fig. 2. (a) Shock velocity history in the quartz standard measured by VISAR (solid red curve). The average shock velocity U_{Qz} used for impedance matching is obtained by integrating $D_{Qz}(t)$ over the corrected time interval $F/\Delta t_{Al}$ (shaded region). (b) The time-modulation factor F of six different the

quartz and aluminum EOS model combinations.

The average shock velocity in aluminum, $<U_{Al}>$, was calculated from the measured step thickness h_{Al} and the transit time $\Delta t_{Al} = t_2 - t_1$. The in-situ shock velocity in the quartz standard was determined from the VISAR fringe shifts using 1.54 as the refractive index, as shown in Fig. 2(a). In laser-driven experiments, shocks are typically non-steady. To apply impedance-matching analysis we corrected the measured average velocities using the method developed by Duan *et al.* [40]. This method introduces a time-modulation factor F to relate the average shock speed in the driver (Al) to an appropriate time-averaged velocity in the standard (quartz) derived from its continuous velocity history. To avoid reliance on a single equation-of-state model, the sensitivity of the correction factor F was evaluated using six combinations of aluminum (PIMC, SESAME 3711, SESAME 3719) and quartz (SESAME 7385, SESAME 7386) tables. The resulting F factors vary from 0.99 to 1.06, as shown in Fig. 2(b). The mean value $F = 1.03$ is adopted, and the model-induced spread is added in quadrature to the velocity uncertainty. The equivalent quartz velocity for impedance matching, $<U_{Qz}>$, was then obtained by averaging $D_{Qz}(t)$ over the corrected time interval $\Delta t_{Al} / F_{Al\text{-}Qz}$:

$$< U_{Qz} >= \frac{1}{\Delta t_{Al} / F_{Al\text{-}Qz}} \int_{t_1}^{t_1 + \Delta t_{Al}/F_{Al\text{-}Qz}} D_{Qz}(t) dt \quad (1)$$

Results for two shots are summarized in Table I. The measured transit times of Al steps were 1.818 ns and 1.794 ns, corresponding to average shock velocities of 65.17 km/s and 66.36 km/s, respectively, with uncertainties below 0.7%. This level of precision was achieved through a combination of a relatively thick aluminum step, which increased the transit time and reduced the relative timing uncertainty, and the high-accuracy measurement of the step height. The corresponding velocities in quartz were 67.16 ± 0.30 km/s and 68.58 ± 0.30 km/s. The quoted uncertainties combine the timing uncertainties from the two VISAR channels and the uncertainty associated with the non-steady wave correction, including the model spread of F. The relative precision of the velocity measurement is better than 0.5%, meeting the level required to distinguish between competing EOS models in this pressure regime.

TABLE 1 Summary of shot parameters and measured shock velocities. E_{laser} is the total laser energy. h_{Al} is the thickness of the aluminum step. Δt_{Al} is the measured shock transit time across the step. U_{Al} is the average shock velocity in aluminum. U_{Qz} is the equivalent average shock velocity in quartz obtained from the non-steady wave correction.

Shot	E_{laser} (kJ)	h_{Al} (μm)	Δt_{Al} (ns)	$<U_{Al}>$ (km/s)	$<U_{Qz}>$ (km/s)
316	123.9	118.48±0.12	1.818±0.012	65.17±0.44	67.16±0.30
318	132.9	119.04±0.14	1.794±0.012	66.36±0.45	68.58±0.30

The aluminum Hugoniot states were determined via impedance-matching (IM) analysis using quartz as the standard. We adopted the quartz principal Hugoniot from the first-principles molecular dynamics (FPMD) calculations by Sjöstrom and Crockett [41], which aligns with experimental data up to ~60 Mbar [11]. The pressure–particle velocity (P-u) relation from this EOS is shown as the solid blue line in Fig. 3. Since the shock impedances of aluminum and quartz are closely matched in this pressure range, we assumed a linear shock-velocity–particle-velocity relation for aluminum, $D_{Al} = U_{Al} \cdot a$, and approximated the release path from the quartz state by a mirror Hugoniot, $P = a\,(U_{Al}/a - u)^2$. The intersection of this mirror line with the quartz Hugoniot defines the quartz shock state (u_{Qz}, P_{Qz}) consistent with the measured average velocities $<U_{Al}>$ and $<U_{QZ}>$. From this intersection, the coefficient a and thus the aluminum Hugoniot state (u_{Al}, P_{Al}) are obtained. The derived aluminum P-u curve and its mirror are plotted as dashed red lines in Fig. 3. The close impedance match between Al and quartz validates the use of the linear D-u and mirror approximations over the limited range of this analysis [30]. Preheating by M-band X-rays from the

gold hohlraum was assessed through radiation-hydrodynamics simulations and found to be negligible, with an estimated change in compression ratio of less than 0.3% (see Supplementary Material).

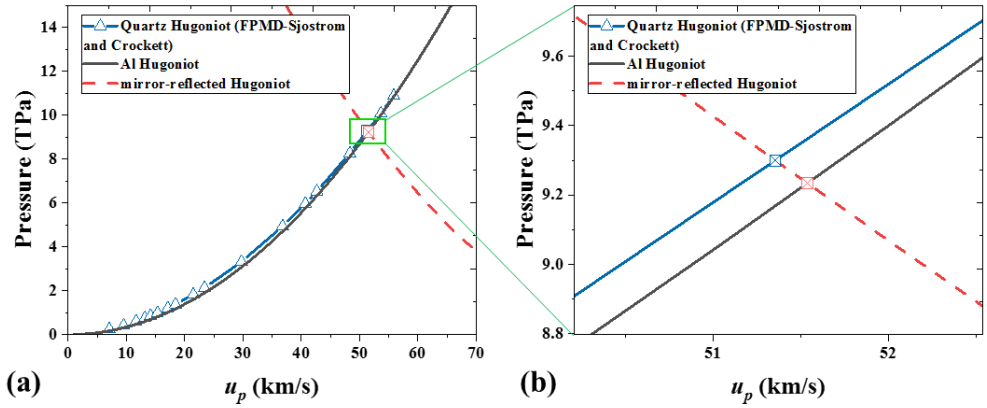


Fig. 3. Impedance-match analysis in the pressure-particle velocity (P-u) plane. (a) Principal Hugoniot of quartz (solid blue line) from first-principles molecular dynamics (Sjöstrom & Crockett). The mirror line (dashed red) for aluminum is constructed assuming a linear D-u relation. Their intersection gives the matched state (u_{Qz}, P_{Qz}), from which the aluminum Hugoniot state (u_{Al}, P_{Al}) is derived. (b) Expanded view showing the close impedance match between aluminum and quartz.

Through impedance-matching analysis using quartz as the standard, we obtained two Hugoniot points for aluminum at pressures of 8.90 ± 0.07 TPa (89.0 Mbar) and 9.29 ± 0.08 TPa (92.9 Mbar), with corresponding compression ratios ρ/ρ_0 of 4.47 ± 0.17 and 4.58 ± 0.18. The complete analysis results are summarized in Table II. Our two new Hugoniot points are plotted in Fig. 4 alongside existing data and theoretical models. The present data, at 89 and 93 Mbar, reach a pressure regime previously accessible only via underground nuclear tests. Crucially, our uncertainty is significantly lower than that of the nuclear test data. In previous impedance-matching measurements at these pressures, iron was often used as the standard material. However, the iron Hugoniot has not been experimentally validated above ~30 Mbar [42], and its large impedance mismatch with aluminum makes the mirror-line approximation unreliable, introducing additional uncertainty. In the present work, quartz was chosen as the standard because its Hugoniot is experimentally constrained up to ~60 Mbar, providing a well-validated reference for the analysis.

TABLE 2 Impedance-matching results for the two shots. u_{Al} is the particle velocity, P_{Al} is the pressure, ρ_{Al} is the density, and ρ/ρ_0 is the compression ratio of shocked aluminum.

Shot	u_{Al} (km/s)	P_{Al} (TPa)	ρ_{Al} (g/cm^3)	ρ/ρ_0
316	50.61±0.39	8.90±0.07	12.08±0.47	4.47±0.17
318	51.86±0.39	9.29±0.08	12.36±0.49	4.58±0.18

Crucially, theoretical models diverge most strongly in the pressure range dominated by inner-shell ionization effects, approximately 50–200 Mbar. First-principles approaches that resolve electronic shell structure predict a softening of the Hugoniot as successive electron shells become ionized. The extended first-principles molecular dynamics (ext-FPMD) method by Zhang [33] retains the Kohn–Sham orbital description for valence electrons while treating high-energy electrons as plane waves, thus preserving shell information at manageable computational cost. The stochastic density functional theory (SDFT) approach [43] uses stochastic orbitals to efficiently sample the electronic states at elevated temperatures, also capturing shell effects without empirical parameters. Both methods give a compression ratio of about 4.45 near 90 Mbar, where L-shell electrons undergo

significant ionization. Similarly, the Hartree–Fock–Slater model combined with charged hard spheres (HFS+CHS) [30] treats bound and continuum electrons separately within a self-consistent field framework, thereby incorporating shell effects explicitly. This model also predicts a softened Hugoniot, consistent with the ext-FPMD and SDFT results in the 50–200 Mbar range. In contrast, average-atom models lack explicit shell structure. The Thomas–Fermi model with quantum and exchange corrections paired with charged hard spheres (TFC+CHS) [30] treats all electrons as a continuous fluid without resolving individual shells. The SESAME 3711 table, also based on an average-atom framework, similarly omits shell details. Both predict a stiffer Hugoniot with a compression ratio of 4.03 near 90 Mbar, 10% lower than the shell-resolved results. The softening predicted by shell-resolved models arises from the energy consumed by inner-shell ionization. As the shock pressure increases, a fraction of the internal energy is diverted to ionizing L-shell electrons rather than heating the ions, which effectively increases the compressibility of the system. At still higher pressures, shell-resolved models predict a second compression peak associated with complete K-shell ionization, though existing experimental data in that regime lack the precision to resolve this feature.

Our two data points at 89 and 93 Mbar yield compression ratios of 4.47±0.17 and 4.58±0.18, respectively. These values lie well within the band of the shell-resolved models and deviate from the average-atom predictions by 8–10%. Compared with earlier data in this pressure regime, which were derived primarily from underground nuclear tests with uncertainties exceeding 30%, the present results provide the first high-precision benchmark capable of distinguishing between competing theoretical descriptions. This provides direct experimental evidence that L-shell ionization softens the aluminum Hugoniot at ultrahigh pressures and demonstrates that first-principles, shell-resolved equation-of-state models offer higher predictive accuracy in the hundred-megabar regime.

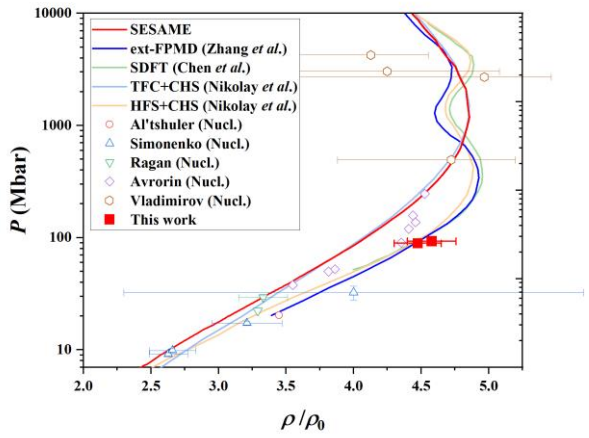


Fig. 4. Principal Hugoniot of aluminum. Our data (solid red squares) are shown with <4% error bars in compression ratios. Existing experimental data: underground nuclear tests (hollow symbols). Theoretical models: shell-resolved predictions include ext-FPMD (Zhang 2016, blue solid), SDFT (Chen 2024, green solid), and HFS+CHS (Kadatskiy 2019, yellow solid). Average-atom models (blue solid) include SESAME 3711 (red solid) and TFC+CHS (light blue solid). Our data clearly favor the shell-resolved models and deviate from the average-atom predictions.

The shell-resolved and average-atom models used in the comparison are equilibrium calculations, whereas our data were obtained under dynamic shock compression, which may in principle involve non-equilibrium effects [44]. A particular concern is the pressure gradient along the loading direction, which thinner samples would reduce but at the cost of amplified interface artifacts. In the present experiment, the aluminum sample thickness (120-190 μm) was chosen to suppress both effects, and the shock transit time (~1.8 ns) is long compared with the relevant

electron–ion equilibration and ionization relaxation timescales. The shocked state is therefore close to local equilibrium, supporting a direct comparison with equilibrium EOS predictions.

The sensitivity of the derived aluminum Hugoniot to the choice of F was further examined. Using the six F values obtained from the EOS combinations described above, we recalculated the Hugoniot compression ratios. As shown in Fig. 5(a), the corresponding Hugoniot compression ratios derived with each F all lie within the experimental error bars. The aluminum Hugoniot data are therefore insensitive to the specific choice of EOS models used for the non-steady correction. We also examined the sensitivity of the results to the choice of quartz standard Hugoniot. The impedance-matching analysis was repeated using three different quartz tables: the FPMD calculations of Sjöstrom and Crockett, SESAME 7386, and SESAME 7385. The FPMD and SESAME 7386 tables agree closely with each other and with experimental data up to ~60 Mbar, whereas SESAME 7385 deviates more noticeably in this pressure range. As shown in Fig. 5(b), even when the most divergent quartz table is adopted, the derived aluminum Hugoniot points shift by less than the experimental uncertainties. The conclusions are therefore robust against the choice of quartz standard within the present precision. The aluminum and quartz shock velocities are provided in Table I so that the impedance-matching analysis can be revisited should the quartz EOS be refined in the future. Both sensitivity studies confirm that the measured softening relative to average-atom models is a robust feature of the aluminum Hugoniot in this pressure regime.

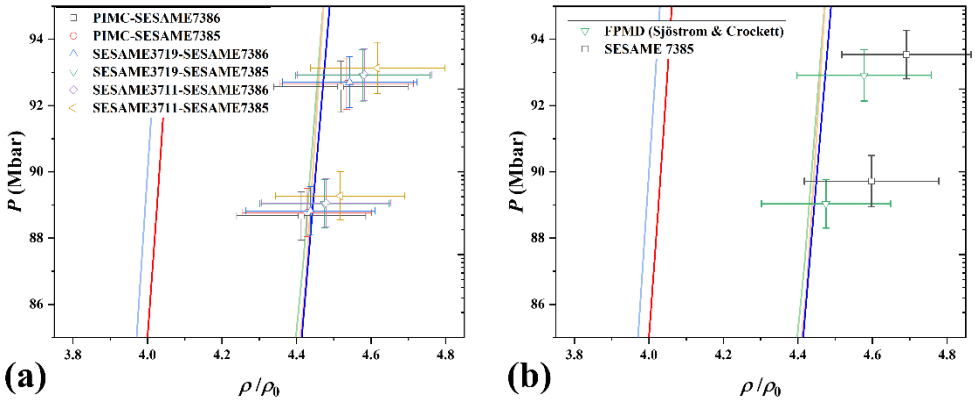


Fig. 5. (a) Sensitivity of the derived aluminum Hugoniot compression ratios to the non-steady correction factor F. The six data points correspond to the F values (0.99–1.06) obtained from the six Al–quartz EOS combinations; all points lie within the experimental error bars. (b) Influence of the quartz reference Hugoniot on the derived aluminum states, comparing the FPMD table with the most divergent SESAME 7385 table.

These results also demonstrate the capability of the present laser-driven platform for high-precision Hugoniot measurements in the 100-Mbar regime. By establishing a reliable benchmark at pressures where inner-shell ionization becomes significant, this work reinforces aluminum's role as an impedance-matching standard for future EOS studies of other materials. Extension of this approach to higher pressures and other mid- to high-Z materials is straightforward.

In summary, we have performed high-precision Hugoniot measurements of aluminum at 89 and 93 Mbar using a laser-driven impedance-matching platform with a quartz standard. The shock-velocity measurement uncertainty is below 0.5%, a factor of three improvement in precision over previous data. The measured compression ratios of 4.47±0.17 and 4.58±0.18 fall within the band of shell-resolved theoretical predictions and deviate from average-atom models by 8–10%. These results quantitatively validate shell-resolved first-principles EOS models against average-atom approximations in the hundred-megabar regime, confirming the critical role of inner-shell ionization physics. Further measurements spanning a wider pressure range would help map the softening trend in detail and are planned for higher-energy laser facilities. These results provide a long-sought high-precision benchmark in the hundred-megabar regime and confirm aluminum as a reliable standard for impedance-matching experiments at hundreds of megabars.

Shell-resolved models further predict a second compression peak due to K-shell ionization above ~300 Mbar. Accessing this regime would require next-generation laser facilities, and the methodology demonstrated here offers a viable path for such future studies.

References

[1] Hirose K, Sinmyo R and Hernlund J 2017 *Science* **358** 734–738
[2] Millot M, Zhang S, Fratanduono D E *et al.* 2020 *Geophys. Res. Lett.* **47** e2019GL085476
[3] Yang F H, Zeng Q Y, Chen Bo *et al.* 2022 *Chin. Phys. Lett.* **39** 116301
[4] Kritcher L, Swift D C, Döppner T *et al.* 2020 *Nature* **584** 51-54
[5] Chabrier G and Debras F 2020 *The Astrophys. J.* **917** 4
[6] Hu S X, Goncharov V N, Boehly T R *et al.* 2015 *Phys. Plasmas* **22** 056304
[7] He Z Y, Zhang Q L, Liu H F *et al.* 2021 *Phys. Rev. B* **103** 134107
[8] Fernandez-Pañella A, Millot M, Fratanduono D E *et al.* 2019 *Phys. Rev. Lett.* **122** 255702
[9] Gaffney J A, Hu S X, Arnault P *et al.* 2018 *High Energy Density Physics* **28** 7-24
[10] Zhao Y H, Wang L F, Zhang Q L *et al.* 2025 *Chin. Phys. B* **34** 036401
[11] Marshall M C, Lazicki A E, Erskine D *et al.* 2019 *Phys. Rev. B* **99** 174101
[12] Jia G, Zhao Y H, Ye J J *et al.* 2025 *High Power Laser Sci. Eng.* **13** e86
[13] Wang P, Zhang C, Jiang S E *et al.* 2021 *Matter Radiat. Extremes* **6** 035902
[14] Knudson M D, Desjarlais M P and Dolan D H 2008 *Science* **322** 1822–1825
[15] Hicks D G, Boehly T R, Celliers P M *et al.* 2005 *Phys. Plasmas* **12** 082702
[16] Li J, Zhou X M, Li J B *et al.* 2012 *Rev. Sci. Instrum.* **83**, 053902
[17] Celliers P M, Collins G W, Hicks D G *et al.* 2005 *J. Appl. Phys.* **98** 113529
[18] Lin C L, Hou Y, Yuan J M *et al.* 2026 *Chin. Phys. Lett.* **43** 050302
[19] Mitchell A C and Nellis W J, 1981 *J. Appl. Phys.* **52** 3363
[20] Al'tshuler L V, Kormer S B, Bakanova A A *et al.* 1960 *Sov. Phys. JETP* **11**, 573
[21] Knudson M D, Lemke R W, Hayes D B *et al.* 2003 *J. Appl. Phys.* **94** 4420
[22] Knudson M D, Asay J R and Deeney C 2005 *J. Appl. Phys.* **97** 073514
[23] Sjostrom T, Crockett S, and Rudin S 2016 *Phys. Rev. B* **94** 144101
[24] Balazs F R, James R A, David A Y *et al.* 2001 *Phys. Lett. A* **291** 226-231
[25] Ragan, C E 1984 *Phys. Rev. A* **29** 1391–1402
[26] Vladimirov A S, Voloshin N P, Nogin V N *et al.* 1984 *JETP Lett.* **39** 82–85
[27] Trunin R F, Panov N V, Medvedev A B *et al.* 1995 *JETP Lett.* **62** 591–594
[28] Avrorin E N, Vodolaga B K, Voloshin N P *et al.* 1987 *Zh. Eksp. Teor. Fiz.* **93** 613–626
[29] Avrorin E N, Vodolaga B K, Voloshin N P *et al.* 1986 *JETP Lett.* **43** 308–311
[30] Orlov N Y, Kadatskiy M A, Denisov O B *et al.* 2019 *Matter Radiat. Extremes* **4** 054403
[31] Kadatskiy M A and Khishchenko K V 2015 Journal of Physics: Conference Series **653** 012079
[32] Blanchet A, Torrent M, and Clérouin J 2020 *Phys. Plasmas* **27** 122706
[33] Zhang S, Wang H W, Kang W *et al.* 2016 *Phys. Plasmas* **23** 042707
[34] Driver K P, Soubiran F, and Militzer B, 2018 *Phys. Rev. E.* **97** 063207
[35] More R M, Warren K H, Young D A *et al.*1988 *Phys. Fluids* **31** 3059–3078
[36] Zheng W G, Wei X F, Zhu Q H *et al.* 2017 *Matter Radiat. Extremes* **2** 243-255
[37] Yang M S, Xing P F, Wei C F *et al.* 2016 *Opt. Precision Eng.* **24** 2738-2745 (in Chinese)
[38] Wang Z B, Jiang X H, Li S W *et al.* 2013 *High Power Laser Particle Beams* **25** 375 (in Chinese)

[39] Jiang S, Wang F, Ding Y K *et al.* 2019 *Nucl. Fusion* **59** 032006
[40] Liu W, Duan X X, Jiang S E *et al.* 2018 *Phys. Plasmas* **25** 062707
[41] Sjostrom T and Crockett S 2015 *Phys. Rev. B* **92** 115104
[42] Dai J Y, Kang D D, Zhao Z X *et al.* 2012 *Phys. Rev. Lett.* **109** 175701
[43] Chen T, Liu Q R, Gao C *et al.* 2025 *Matter Radiat. Extremes* **10** 057601
[44] Sun L, Chen B, Chen Z J *et al.* 2025 *Matter Radiat. Extremes* **10** 063002